

Optics for the imaging x-ray polarimetry explorer

Brian D. Ramsey,^a Stephen D. Bongiorno^{b,*}, Jeffery J. Kolodziejczak,^a
Kiranmayee Kilaru,^b Cheryl Alexander,^c Wayne H. Baumgartner,^a
Shawn Breeding,^a Ronald F. Elsner,^a Shelley Le Roy,^d Jeff McCracken,^c
Ikuyuki Mitsubishi,^e Stephen L. O'Dell^b, Steven D. Pavelitz,^a
Jaganathan Ranganathan,^b Javier Sanchez,^d Chet O. Speegle^b,^a
Nicholas Thomas,^a Bruce Weddendorf,^f and Martin C. Weisskopf^a

^aNASA Marshall Space Flight Center, Huntsville, Alabama, United States

^bUSRA, Marshall Space Flight Center, Huntsville, Alabama, United States

^cLinc Research, Marshall Space Flight Center, Huntsville, Alabama, United States

^dESSCA, Marshall Space Flight Center, Huntsville, Alabama, United States

^eNagoya University, Nagoya, Japan

^fWeddendorf Design, Huntsville, Alabama, United States

Abstract. The Imaging X-ray Polarimetry Explorer, a NASA small explorer mission, will be the first mission dedicated to x-ray polarimetry. The payload consists of three identical telescopes, each comprising a mirror module assembly (MMA) with a polarization-sensitive detector at its focus. We describe all aspects of the MMA, from initial optical and mechanical design considerations to meet program requirements through mirror shell fabrication, mirror shell integration and module assembly, environmental testing, x-ray calibration, and on-ground and on-orbit alignment. © The Authors. Published by SPIE under a Creative Commons Attribution 4.0 International License. Distribution or reproduction of this work in whole or in part requires full attribution of the original publication, including its DOI. [DOI: [10.1117/1.JATIS.8.2.024003](https://doi.org/10.1117/1.JATIS.8.2.024003)]

Keywords: x-ray astronomy; grazing-incidence optics; polarimetry.

Paper 21129 received Oct. 14, 2021; accepted for publication Apr. 14, 2022; published online May 19, 2022.

1 Introduction

The Imaging X-ray Polarimetry Explorer (IXPE) will be the first mission designed specifically for x-ray polarimetry.^{1,2} It will operate over the 2 to 8 keV energy band and will measure polarization from most classes of x-ray sources including supernova remnants, stellar mass black holes, neutron stars, and active galactic nuclei. IXPE, a NASA-funded small explorer mission, with substantial contributions from the Italian Space Agency (Agenzia Spaziale Italiana [ASI]), was launched on December 9, 2021, into an equatorial orbit of altitude 600 km. This orbit ensured passage over an Italian-contributed ground station in Malindi, Kenya, every 95 min for frequent data downloads (typically 8 per day). During its 2-year baseline mission, IXPE will look at ~35 science targets in year 1 with follow-on observations in year 2.

The IXPE payload consists of three identical telescopes, each comprising a mirror module assembly (MMA), fabricated by NASA at the Marshall Space Flight Center (MSFC), and a detector unit, contributed and fabricated by Italy (see Fig. 1). The MMAs, each of which contain 24 concentric-nested Wolter-1 mirror shells, provide for imaging and flux concentration, effectively reducing the instrument background to negligible levels for most observations [on orbit, IXPE sees <0.5 c/s background per detector (2.25 cm²), five orders of magnitude less flux than from a bright IXPE target]. The detectors, gas proportional counters with electron-tracking capability, provide information on the position, timing, energy, and, uniquely, polarization of incident x-ray photons.

*Address all correspondence to Stephen D. Bongiorno, stephen.d.bongiorno@nasa.gov

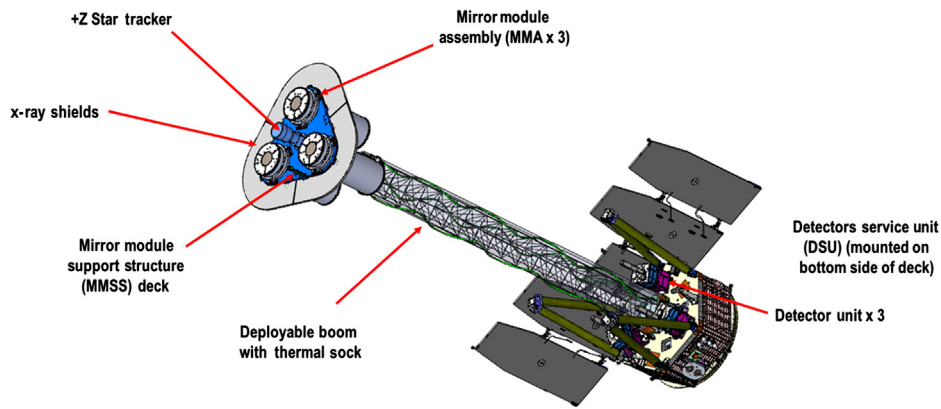


Fig. 1 The IXPE Observatory with the payload deployed.

This publication is focused on the MMAs. In the following sections, the optical, mechanical, and thermal designs are described (Secs. 2.1–2.3, respectively), followed by a description of the process of mirror shell fabrication (Sec. 2.4) and mirror module assembly (Sec. 2.5). Following that, subsequent sections cover MMA environmental testing (Sec. 3), x-ray calibration (Sec. 4), and a discussion of both on-ground and on-orbit telescope alignment (Sec. 5). A brief summary (Sec. 6) concludes the publication.

Further details of the IXPE mission, the detectors, and the science goals are given in a separate publication.³

2 IXPE Mirror Module Assemblies

2.1 Optical Design Requirements and Optimization

The design of the optics assembly must provide the necessary performance, when folded with the detector response, to achieve the top-level science requirements. These so-called Level-1 science requirements flow down to lower levels, with appropriate margins included to arrive at requirements for the optics themselves (Level-4).

For IXPE, early design optimizations and trade studies arrived at the final configuration of three modules, each with 24 concentrically-nested grazing-incidence mirror shells. This configuration was optimized to fit within the fairing of the initially-planned Pegasus launch vehicle (the launch vehicle was later changed to a SpaceX Falcon 9 but after the payload design was complete). Specifically, utilizing three independent mirror module assemblies instead of one larger mirror module permitted a shorter focal length for the given graze angles (dictated by the energy range of interest), which in turn permitted a shorter deployable boom to achieve the focal length on-orbit. Also, having three independent identical telescope systems (each with an MMA and a detector) gave some redundancy against hardware failure and permitted 120 deg detector clocking to mitigate against any systematic effects in the polarization-sensitive x-ray detectors once the relative orientation of the detectors was accounted for.

The final choice of 24 concentrically nested mirror shells per module was designed to give the necessary collecting area and energy response to meet science requirements, within the overall observatory mass budget, based on a mirror shell thickness that would permit an MMA angular-resolution requirement to be met with the assembly procedure planned (see Sec. 2.5). The mirror prescription chosen is the commonly-used Wolter-1 configuration⁴ in which reflections off a parabolic then a hyperbolic surface provide good imaging response off axis. Slightly unusual for an x-ray astronomy mirror system, there was no additional reflective coating on the inside of the mirror shells because the nickel/cobalt surface gave optimum reflectivity for the specific energy range of IXPE (2 to 8 keV). Thus, the additional steps of depositing an optical coating, such as iridium or gold, were avoided.

Table 1 details the parameters of the IXPE mirror module assemblies. Included in the table are the relevant requirements and the actual as-built-and-tested values. A discussion of the slight

Table 1 IXPE Mirror Module Assembly parameters.

Parameter	Value	
Number of mirror modules	3	
Number of shells per mirror module	24	
Focal length	4 m	
Total shell length	600 mm	
Range of shell diameters	162 to 272 mm	
Range of shell thicknesses	0.18 to 0.25 mm	
Shell material	Electroformed nickel-cobalt alloy	
	Requirement	Actual
Effective area per mirror module (average over three modules)	$\geq 183 \text{ cm}^2$ (2.3 keV);	167 cm^2 (2.3 keV);
	$\geq 218 \text{ cm}^2$ (4.5 keV)	197 cm^2 (4.5 keV)
Angular resolution (HPD)	≤ 25 arcsec	19 to 28 arcsec
Field of view	≥ 11 arcmin diameter	12.9 arcmin square
Ghost ray reduction	≥ 100	>200
Module mass (with shields)	≤ 33.5 kg	31.0 kg

shortfall in the effective area and angular resolution is included in the calibration section, in which results are discussed in some detail.

2.2 Mechanical Design

The principal challenge for MMA mechanical design is surviving launch loads while maintaining angular resolution. An accurate assessment of these loads is very important for avoiding overdesigning (or subsequently overtesting) the hardware. Typically, the launch provider gives the expected loads at the observatory interface, which would be propagated to the mirror modules. Clearly, this is an iterative procedure to optimize the mechanical design.

A second requirement is that the mechanical design facilitates the assembly of the mirror module, permitting assembly from the innermost mirror shell outward while not distorting the mirror shell at its attachments point and providing adequate access to bond areas sufficient to withstand launch loads. This requirement is particularly challenging as each mirror module is heavily nested, with just ~ 2 mm between successive shells.

Figure 2 shows the mechanical design of the IXPE MMA with the front end down—its orientation during alignment and assembly (see Sec. 2.5). In order of assembly, the principal components of the MMA are the front spider, central support tube, mirror shells (inner to outer), rear spider, outer housing, and fore and aft thermal shields.

The front spider is the primary structural element, through which the MMA will be mounted onto the mirror module support structure (MMSS) during payload integration at the spacecraft supplier (Ball Aerospace). The central support tube serves as an alignment reference and support structure for components at the rear end of the MMA. Each of the nine spokes of the front spider has a precisely fabricated and positioned comb glued to it. During MMA alignment and assembly, each mirror shell is inserted and glued into the corresponding slot between the tines of each comb, thus attaching the mirror shells to the spokes of the front spider. The spider and combs are fabricated from 17-4PH stainless steel, which has an expansion coefficient close to that of the nickel/cobalt mirror shells. This similarity of expansion coefficients somewhat relaxes thermal control requirements (see Sec. 2.3).

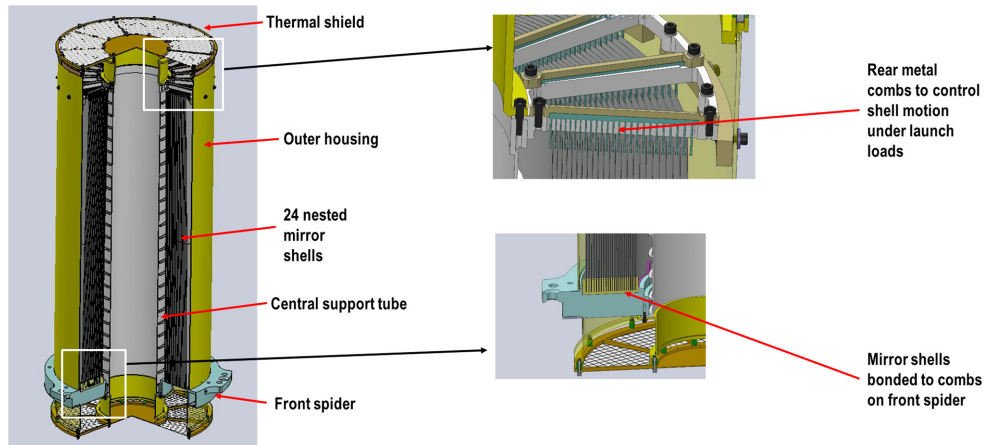


Fig. 2 Schematic showing the mechanical design of an IXPE MMA.



Fig. 3 Rear spider of the MMA.

The rear spider has 18 spokes, each with a metal comb (see Fig. 3). After the 24 shells are glued to the front spider, the rear spider is attached to the central support tube, and its metal combs are aligned such that each mirror shell floats within the corresponding slot between the tines of the rear-spider combs (with a typical gap of 0.22 mm on either side). Unlike the front-spider combs, which hold the mirror shells in place, the rear-spider combs do not touch the shells and merely limit excursions of the shells under launch loads to preclude shell-to-shell collisions. In this way the mirror shells are not over-constrained, as they would be if they were rigidly attached at both ends. To prevent possible marring of the mirror-shell surface and to provide protection against shock and vibration impacts, the rear comb tines have heat-shrink sleeves applied to cushion impacts.

2.2.1 Engineering unit

Early in the program, an engineering unit (EU) of the MMA was fabricated. This was a copy of a flight unit, but populated with only 6 of 24 mirror shells plus 3 mass simulators to duplicate the mass and dynamic response of the missing 18 mirror shells (Fig. 4). The six EU shells, the innermost three and the outermost three, were fabricated using flight mandrels that were then refurbished for the flight mirror fabrication.

The added value of the EU to the program was considerable. It enabled the whole fabrication and assembly program to be verified at an early stage of the project, and handling fixtures and other ground support equipment to be tested. Further, it permitted validation of the optical design through x-ray testing and validation of the mechanical design through environmental testing.

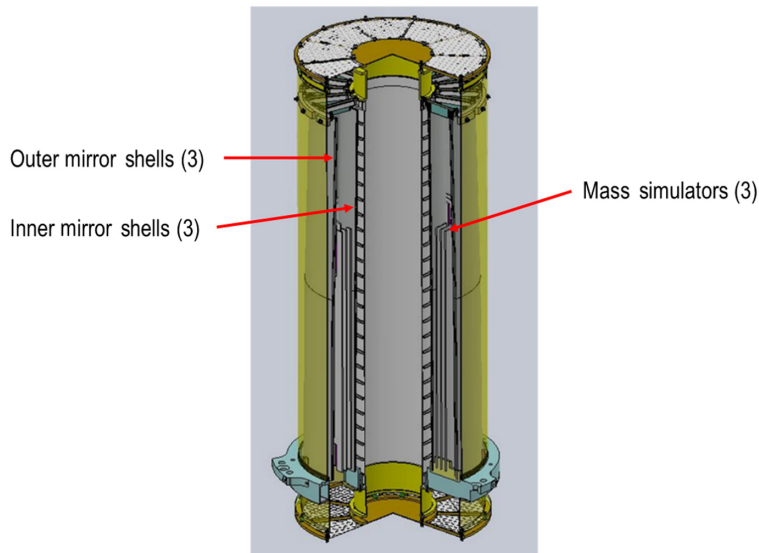


Fig. 4 Schematic of the MMA engineering unit.

In fact, x-ray testing was performed before and after each mechanical and thermal test to confirm that the optical performance had not changed.

During vibration testing, an early failure led to tighter controls on humidity during the bonding process when it was discovered that the epoxy used for shell bonding was sensitive to high humidity during the curing phase. Also, it was found, using high-speed cameras, that the thin mirror shells could become unstable under vibration and behave non-linearly unless tightly constrained. This led to a change in design, in which the number of rear spider spokes was doubled from an original 9 to 18. After a re-build, subsequent testing, interleaved with x-ray tests after each environmental test, confirmed that the new design could handle the test loads without any degradation.

The EU also permitted additional shock tests to establish limits on the number and magnitude of shocks that the flight units could withstand (from multiple firings of the launch locks holding the payload in the stowed configuration). Finally, the EU provided a test system to verify procedures and hardware for MMA calibrations.

2.3 Thermal Design

Thermal requirements for the MMAs are derived from a STOP (structural, thermal, optical performance) analysis of the effects of overall temperature and temperature gradients on the imaging performance of the optics. For this, the MMA finite-element mechanical model is used, temperature gradients are applied, and the resulting model is inputted to a ray-trace program for an assessment of the imaging performance. Temperature gradients along the MMA axis and across the MMA diameter as well as changes in the overall operating temperature of the module were investigated. The most critical requirement was found to be circumferential gradient around individual shells (i.e., with one side of a shell having a different temperature than the other side), and a maximum of 2°C was set to maintain imaging performance. Figure 5 (left) shows figure deviations on the inside of an individual mirror shell distorted by this temperature difference. Figure 5 (right) gives the net imaging distortion [in terms of half-power diameter (HPD)] per shell under this condition. Other thermal requirements established were an axial gradient of less than 5°C per mirror shell and an operating temperature of $20 \pm 5^{\circ}\text{C}$ for each of the mirror shells (acknowledging that the inner shells will run slightly cooler than the outer ones), the latter is a fairly loose requirement aided by matching the thermal expansion coefficient of the main spider and combs to that of the mirror. The combined effect for the complete mirror module, if all of these requirements are at their limit, is a distortion of ~ 7 arcsec HPD, which adds in quadrature to the native MMA resolution, increasing it by less than 1 arcsec.

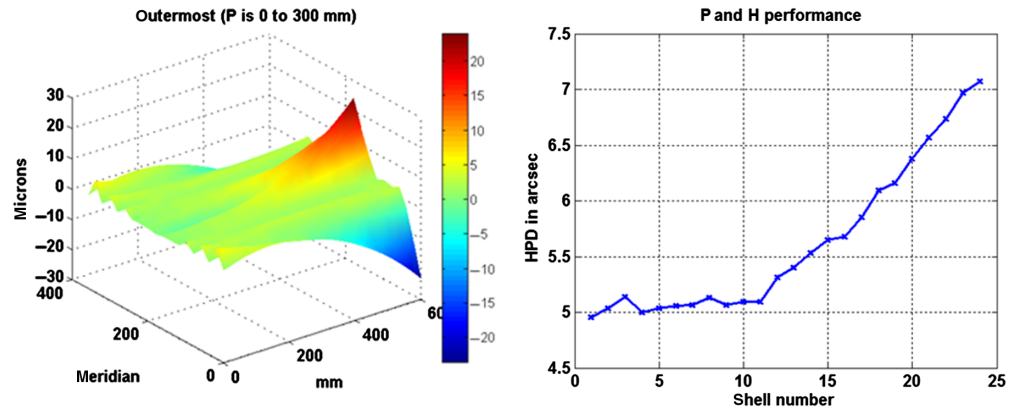


Fig. 5 Mirror shell distorted by a circumferential temperature gradient of 2°C (left); resulting x-ray angular resolution (HPD) as a function of shell number (24 = outer shell).



Fig. 6 A thermal shield mounted on the rear of a flight mirror module assembly. Visible just below the shield is a band heater (one of three at each end) that maintains the MMA within its operating temperature range.

To maintain temperature, the MMA is equipped with six heaters, arranged in two circumferential bands of three heaters each, located ~ 30 mm from the ends of the MMA (see Fig. 6) and circumferentially wrapped in multilayer insulation (MLI). To minimize heat loss from the ends of the MMA, without losing low-energy x-ray response, the MMA apertures are covered with thermal shields, contributed by Nagoya University, Japan. These consist of a $1.4\text{-}\mu\text{m}$ -thick polyimide film coated with ~ 50 nm of aluminum and are supported on a 97.5% transparent stainless-steel mesh (Fig. 6). The transmission of a pair of these shields, fore and aft, is 76% at 2 keV, 88% at 3 keV, 91% at 4 keV, and 94% at 8 keV.

2.4 Mirror Shell Fabrication Process

The IXPE mirror shells are fabricated from an electroformed-nickel replication (ENR) process. In this approach, a master or mandrel is produced for each shell diameter, and a thin mirror is replicated from it through electroforming. The mirror shell is separated from the mandrel by differential thermal contraction in a chilled water bath, in which the aluminum mandrel shrinks away from the nickel alloy shell. The ENR process has been used on many programs over the years—at MSFC for HERO,⁵ FOXSI,⁶ and ART-XC⁷ and elsewhere for such missions as XMM-Newton⁸ and eROSITA.⁹

The attraction of the ENR process is that it is a relatively inexpensive way to produce medium-angular-resolution optics and, once a mandrel has been fabricated, multiple copies can be easily electroformed, making it ideal for situations in which multiple, identical mirror

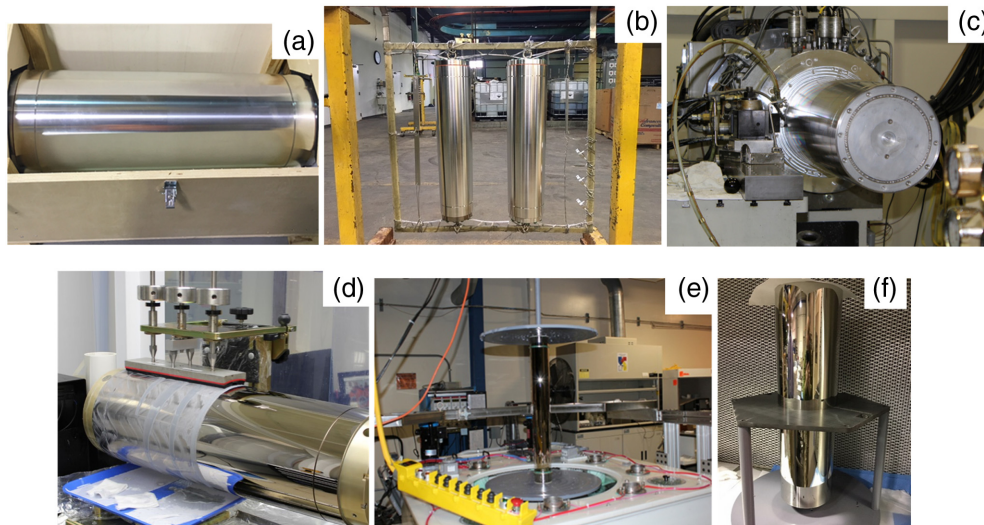


Fig. 7 The ENR process: (a) mandrel blank fabrication; (b) electroless nickel coating; (c) diamond turning; (d) lap polishing; (e) mirror shell electroforming; and (f) released shell in handling fixture.

modules are required. Also, for the typical Wolter-1 geometry, the parabolic and hyperbolic segments can be manufactured as a single piece, greatly simplifying the alignment.

The production of the mandrel involves machining an aluminum bar to near final shape and size [see Fig. 7(a)] and then coating it with electroless nickel (nickel-phosphorous), a durable material that can be accurately figured and polished [Fig. 7(b)]. Figuring is typically performed using single-point diamond turning [Fig. 7(c)] to achieve the micron-level accuracy necessary for 20-arcsec-resolution optics. After turning, conventional lap polishing is utilized [Fig. 7(d)] to achieve a surface roughness of 0.5 nm rms, which is necessary to minimize scattering at the x-ray wavelengths of interest.

MSFC uses a nickel/cobalt ($\sim 80/20$) alloy for its mirror shells. This material has low ductility, which makes it less susceptible to distortion during electroforming, release, and subsequent handling. A typical IXPE shell of thickness 200 μm is electroformed in about 11 h [Fig. 7(e)]. After the shell is released in cold water, it is dried and put in a handling fixture to wait for installation [Fig. 7(f)].

2.5 Assembly of Mirror Modules

Assembling a mirror module is challenging as thin mirror shells can be easily distorted at attachment points, leading to performance degradation. One way to reduce this effect is to float the mirror shell in a groove, into which low-shrinkage epoxy is injected, thereby preserving, for the most part, the shell's natural shape. For past programs at MSFC, a mirror shell has typically been supported on pins that can be used to manipulate it and center it in the spider comb grooves for bonding.¹⁰ For IXPE, however, the mirror shells are too thin for this approach, and they distort at the support points. This distortion would then be incorporated into the nearby bonded joints, degrading angular resolution. To avoid this, the approach adopted for IXPE was to hang the mirror shells from a series of wires, so any distortions due to the mirror support are at the opposite end of the shell from the bonded joints.

Figure 8 shows the design (left panel) of the IXPE MMA alignment and assembly station, which has a graphical interface for software-controlled optimization of the alignment of each shell. To allow for parallel production of four IXPE MMAs (three flight and one flight spare), there were four alignment and assembly stations, located in an ISO-7 (Class-10k) cleanroom to help satisfy cleanliness requirements.

The IXPE alignment and assembly system holds each successive shell by hanging it via a set of nine support wires: three wires can be adjusted by piezo actuators and the other six serve as mass off-loaders. A rotary table with three high-precision proximity sensors rotates while the

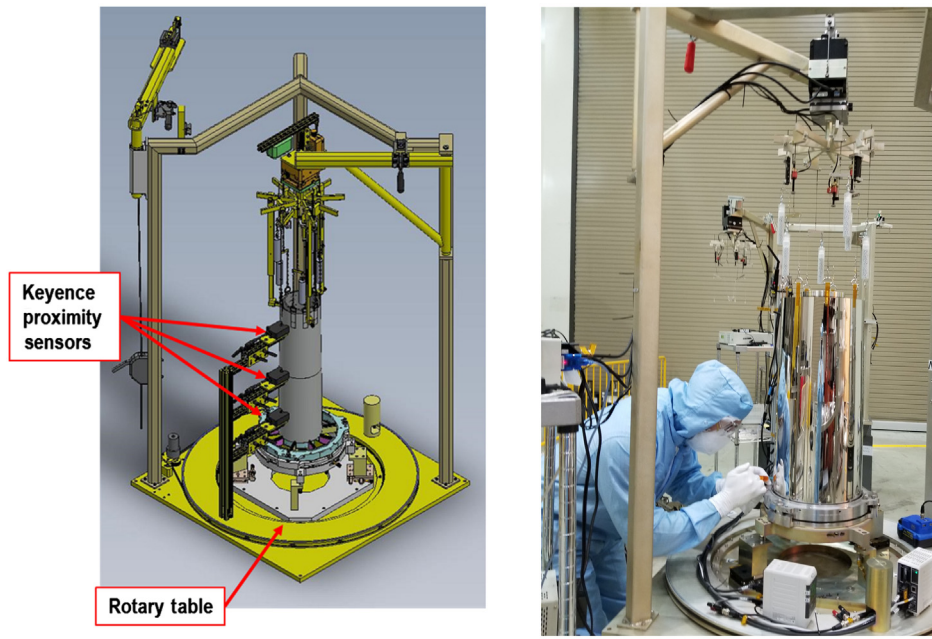


Fig. 8 Alignment and assembly of the IXPE mirror modules. Left image is a schematic representation of an MMA alignment and assembly station. Right image shows the bonding of an IXPE mirror shell.

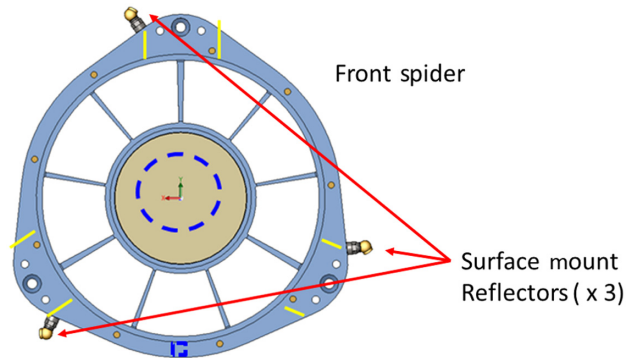
sensors measure radial displacements of the external surface of the mirror shell near the intersection and near the two ends of the shell. Software acquires the displacement data as a function of rotation angle and fits those data to various curves, calculating parameters (shell center, tilt, and circularity) that aid in alignment and performance optimization. Custom software analyzes these calculated parameters and adjusts the three non-offloaded hanging points to obtain the best alignment and centering of the mirror shell. This computer-controlled process typically converges in about 20 min.

Once this is done, wire shims ranging in thickness from 0.14 to 0.18 mm are inserted between the outside surface of the shell and the opposing surfaces of the comb slots. See Fig. 2 for an illustration of how the shells are bonded to slots in the combs. The shims serve several purposes: to ensure that a nominal gap exists between the shell and the comb slots so that epoxy can effectively wick into the joints, to ensure that a nominal gap exists so that joints will achieve nominal strength, and to allow for radial adjustment of the shell shape at each spoke, which may be used to improve the shell angular resolution. When the performance is optimized, the operator injects epoxy into the front-spider comb slots (see Fig. 8; right), and the assembly is left to cure overnight.¹¹

There were multiple goals for the shell assembly process. One was to center the optical node of each shell within $30\ \mu\text{m}$ of the MMA optical axis to conservatively satisfy a $50\ \mu\text{m}$ requirement on node position determination for overall MMA alignment on the spacecraft. Another goal was for each shell optical axis tilt to be within 25 arcsec of the MMA optical axis to ensure that the shells would float in the center of the rear comb grooves. The third goal was to use the proximity sensor data that were used to align the shells to continually calculate a cumulative performance prediction for each MMA before each shell was bonded in place. If the alignment of a particular shell did not meet a 20 arcsec goal, conservatively set to ensure a 25 arcsec module performance, the cumulative performance calculation was used to decide whether to bond the shell in place or rework the alignment. Mean shell alignment parameters for shells 2 to 24 in each MMA are reported in Table 2. It can be seen from the table that centering, tilt, and circularity contribute a small amount to the overall module angular resolution, as all parameters in Table 2 contribute to the total error in quadrature. By far the largest component in the table is the calculated parameter Delta-Delta-R (DDR). This is a measure of the change in slopes of the parabolic and hyperbolic segments as a function of azimuth around the mirror shell. It is calculated from

Table 2 Shell alignment summary.

MMA	Centering (μm) [arcsec HPD]	Tilt (arcsec) [arcsec HPD]	DDR * 2 [arcsec HPD]	Circularity (μm) [arcsec HPD]
MMA1	14.8 ± 19.6 [0.92]	10.4 ± 12.4 [3.0E-3]	16 ± 5	26.0 ± 11.0 [2.4]
MMA2	18.9 ± 10.1 [1.1]	10.1 ± 6.1 [2.5E-3]	16 ± 4	40.7 ± 14.8 [4.0]
MMA3	16.0 ± 8.4 [0.88]	9.2 ± 6.2 [2.7E-3]	15 ± 4	33.9 ± 11.7 [3.2]

**Fig. 9** SMRs mounted on front spider.

the Keyence circularity sensor data and is a measure of low-frequency distortions in the shell, which dominate imaging performance. This number, averaged over the module, provides the best indicator of shell performance, and its running average is constantly monitored during assembly to meet the 25 arcsec HPD performance requirement.

The reported values are magnitudes and represent the alignment state of the shells an average of 15.8 h after bonding (to allow for any epoxy shrinkage), immediately before installation of the next larger shell. Shell 1 is excluded because, after shell 1 bonding, the MMAs are realigned on the alignment station to remove shell 1 alignment errors. These alignment parameter averages are shown to quantify shell alignment results and have not been weighted by shell effective area. The focal plane angular error due to each alignment parameter (arcsec HPD, shown in brackets) has been weighted by the shell geometric effective area to show the relative contribution of each parameter to the total MMA HPD.

An important component of the assembly process is measuring the position of the MMA optical node with respect to surface mount reflectors (SMRs), which are mounted around the front spider (see Fig. 9). These SMRs are later used to position each MMA precisely on the observatory to allow for coalignment of each telescope. The optical node is the central point of the optic, near the intersection plane between the hyperbolic and parabolic segments. The precise location of the SMRs with respect to the node is measured during module assembly. The resulting node-position information is passed to the spacecraft integrator (Ball Aerospace) for use during MMA integration into the observatory to ensure correct alignment.

3 Environmental Testing

All hardware must undergo environmental testing to qualify it for launch. For vibration testing of delicate optics, which can be harmed by unnecessarily high loads, this could involve testing to the maximum expected launch loads plus 3 dB (protoflight levels) or just the maximum expected launch loads (acceptance level). Other items, particularly mechanisms and electronics, would typically have higher-load minimum workmanship test requirements.

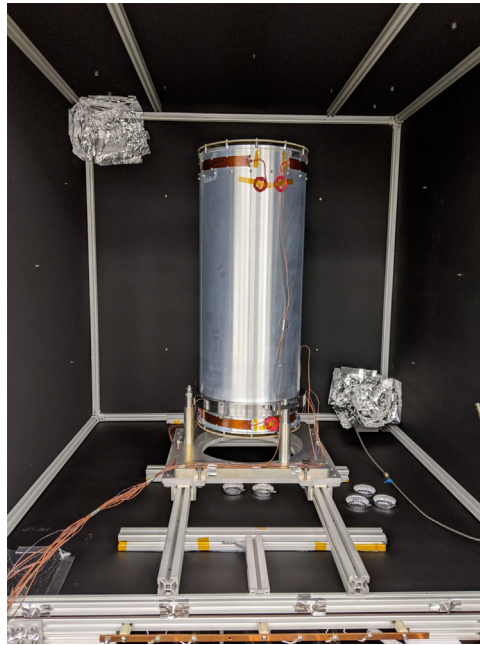


Fig. 10 Flight MMA inside thermal vacuum chamber.

One of the four IXPE MMAs (three flight units plus an identical spare unit) was subject to vibration and acoustic testing and thermal cycling (Fig. 10). The other three, including the spare unit, went through vibration testing and thermal cycling only. Two flight MMAs were vibration tested to protoflight levels (60 s per axis) and two (one flight unit plus the spare unit) were tested to acceptance levels (also 60 s per axis). Additional vibration, shock, acoustic, and thermal tests were carried out later at the observatory level.

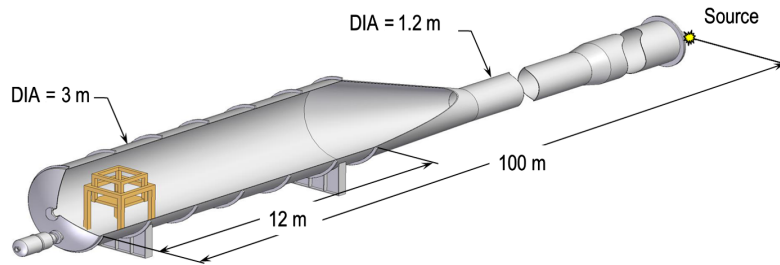
Thermal (vacuum) cycling was performed over the survival temperatures of the MMA, which are 0°C to 40°C. These are the temperature extremes that can be safely handled without any permanent changes in performance. They were derived from finite-element analysis and confirmed through testing of the MMA engineering unit. These thermal cycles were run without multilayer insulation on the MMA housings (to shorten the cycle time) but with the thermal shields installed. Six hot-cold cycles, lasting ~36 h each, were run for each MMA. After each environmental test (including at the observatory level) a detailed inspection was performed on each MMA, including photographic records of every bond joint and every shell position in the rear spider combs. No discrepancies were found, and all MMAs passed environmental testing.

4 Calibration

Precise calibration of x-ray telescopes is very important for subsequent analysis of on-orbit data. IXPE calibrations consisted of detailed detector calibrations in Italy and detailed MMA calibrations in the United States.

MMA calibrations, performed after all MMA environmental testing, were carried out at the MSFC Stray Light Test Facility (SLTF), which features a 100-m vacuum beamline with x-ray source assemblies at one end and a 12 m × 3 m test chamber at the other (see Fig. 11). The MMA under calibration, with thermal shields attached, was mounted in the test chamber atop a hexapod which enabled precise linear control in all axes and precise angular control in tip and pan. Beyond the MMA, at an image distance of 4.17 m (the finite-conjugate focal length of the MMA for a 100-m source distance), were facility detectors to measure the MMA response. These consisted of a fast silicon drift detector (SDD) with known effective area and a charge-coupled device (CCD) camera with fine (13.5 μm) pixels for accurate measurements of the MMA point spread function.

It is important to understand that the response of the MMA at a finite-source distance differs from that on orbit, where sources are effectively at an infinite distance. This is because the optic


Fig. 11 MSFC SLTF.

is designed for a parallel beam of incident x-rays, whereas the beam is divergent at the SLTF, coming from a point source just 100 m away. This has the effect of increasing the graze angles so that the effective collecting area differs from what it would be on-orbit as does the mirror's energy response (which is graze-angle dependent). The effect is dependent upon focal length and source distance, being largest for a short source distance and a large focal length. It is typically calculated by ray tracing. For IXPE, the on-axis correction is +22% at 2 keV and +18% at 8 keV and must be applied to the facility-measured effective area.

Calibration measurements were made for on- and off-axis effective areas and angular resolutions. Effective area measurements were made using two identical silicon drift detectors with accurately known effective areas. One of these was placed at the entrance aperture of the MMA under test, and the other was placed at the focus. The ratio of the count rates multiplied by the known effective area of the SDD gave the MMA effective area. The measured effective areas for the three flight MMAs, corrected to infinite source distance, along with a best-fit model curve, is shown in Fig. 12 using continuum radiation from a molybdenum-target x-ray source.

The measured effective areas were about 10% lower than the MMA-level requirement (183 cm² at 2.3 keV and 217 cm² at 4.5 keV) and about 16% lower than expected from modeling, possibly due to a variety of factors including slight misalignment of the spokes in the front and rear spiders and the thermal shields. The Level-1 requirement that sets the effective area is the observatory polarization sensitivity. This is a complex dependency of the MMA effective area and detector characteristics (quantum efficiency and response to polarization) and has a significant margin built into its requirement flow-down, equivalent to 20% in the MMA effective area. Because of this, the driving Level-1 polarization sensitivity requirement is still met.

The HPD of each MMA was measured using a CCD camera at the focus of the optic, with filtered x-ray sources producing lines at nominally 2.3 keV (Mo-L) and 4.5 keV (Ti-K). The detector collection region used for this measurement was chosen to be the same as that used for the effective area, i.e., a circle of diameter 8 mm, which is approximately 16 times the

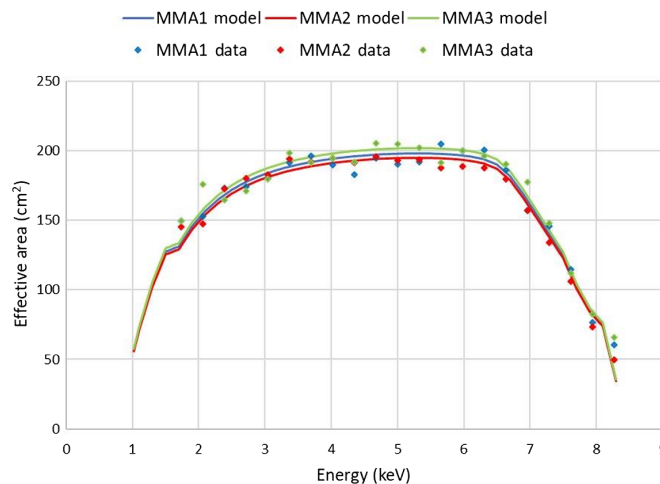

Fig. 12 Measured effective area of flight MMAs corrected to infinite source distance.

Table 3 Measured angular resolutions of flight MMAs.

	MMA1		MMA2		MMA3	
Energy (keV)	2.3	4.5	2.3	4.5	2.3	4.5
HPD (arcsec)	19	19.9	25	26	27.6	28

expected MMA HPD [subsequent CCD measurements during calibration confirmed that this (8 mm) diameter contained >98% of the flux at 2.3 keV and >95% of the flux at 6.4 keV]. Flat fields, taken immediately before and after the measurements, were used to subtract offsets and noise contributions in individual pixels. The diameter containing half the flux within the measurement region was then determined and converted to an angle using the measured image distance (~ 4.17 m) for the 100-m object distance at the SLTF. The results are shown in Table 3. A more detailed account of the MMA imaging performance is given in a separate publication.¹¹

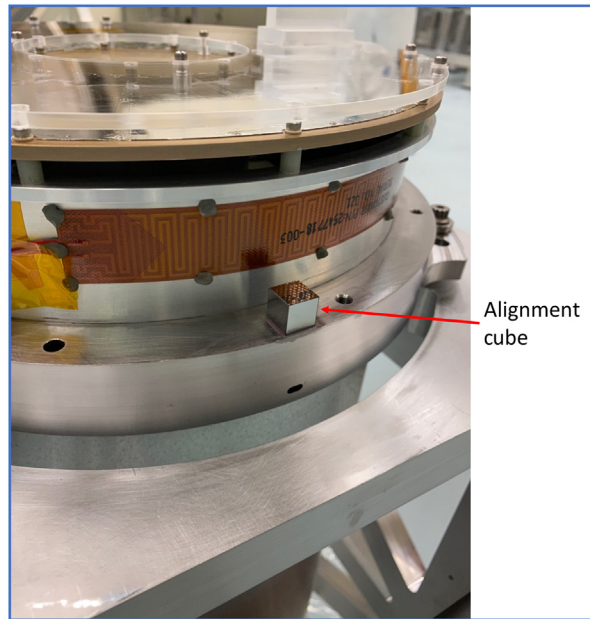
The angular-resolution requirement for each MMA was ≤ 25 arcsec HPD, so two of the MMAs fall just outside this value (one marginally). Thus, the predictions from the shell assembly (Sec. 2.5) underestimated the final HPD value for MMA2 and MMA3. In searching for the source of increased optical distortion in these modules, measurements ruled out damage from environmental testing, misalignment stress between the thermal shields and the optical module, distortion induced by the calibration fixture, and stress induced by the bolted interface between the alignment station and the optical module. Untested potential sources of distortion include misalignment stresses between the central support tube, the rear spider, and the outer housing (installed after all of the shells were glued in place) which, because of the large lever arm of the central support tube can ultimately distort the front spider, and front spider distortion caused by the MMA handling fixture that was made permanent when either the outer housing or front thermal shield supports were bonded in place. For future builds, the source of this degradation in MMA2 and MMA3 should be understood. This is still being investigated and will be reported in a future paper. However, the Level-1 system angular resolution requirement, set by IXPE science, is 30 arcsec (three telescopes averaged) and factors in not only the MMA native resolution but also detector effects and the performance of the aspect system. Factoring in these, the final (pre-launch) system angular resolution was estimated to be 27.9 ± 0.5 arcsec HPD, within requirements. After launch and during the 1-month observatory commissioning, analysis of data from a celestial point-source target showed a system angular resolution of 28.2 arcsec, in very good agreement with pre-launch estimates.

In addition to the above measurements, “ghost” rays were measured at a series of off-axis angles. These rays are from sources outside the normal field of view that undergo a single reflection (instead of two) typically off the hyperbolic mirror segment and end up in the flight detector, thereby contributing an additional background component. For point source measurements, these are not an issue; for weak extended sources, in which there are very bright point sources just outside the field of view, this can potentially degrade the telescope sensitivity. IXPE has requirements on the amount of such stray radiation, controlled by heavily nesting the mirror shells to block off radiation paths and verified as part of the x-ray calibration. The requirement calls for the flux from any source outside the field of view to be reduced by at least a factor of 100 over what that source would be on axis. This requirement is driven by a planned observation of molecular clouds near the Galactic Center that are weak sources of x-rays but have bright x-ray sources nearby just out of the field of view. Simulations show that, above 1 deg off axis, it is not possible for singly reflected rays to reach the focal plane. Therefore, during calibration, data were taken at 2.3 keV up to and including this off-axis angle. The ghost-ray attenuation factors, which are the ratio of on-axis to off-axis effective areas that were measured as a function of off-axis angle for the three flight MMAs, are shown in Table 4. It is clear that the MMAs satisfy the factor of ≥ 100 requirement.

An important measurement during calibration is that of the alignment cube which is mounted atop each MMA (Fig. 13). This cube is used to define the x-ray axis such that each MMA can be co-aligned on the observatory and aligned with the star tracker. This ensures that the MMAs are mounted in such a way to ensure maximum throughput. The alignment of the cube is measured

Table 4 Ghost ray measurements as a function of off-axis angle (see text).

MMA	0.2 deg	0.4 deg	0.6 deg	0.8 deg	1.0 deg
MMA1	260	665	865	1139	1215
MMA2	233	610	854	997	1023
MMA3	242	643	876	1164	1112

**Fig. 13** Optical alignment cube mounted to the MMA front flange.

during calibration by aligning the MMA in x-rays and then reflecting a laser off the cube at 100 m to measure the precise offset of the cube normal with respect to the x-ray axis.

5 MMA Alignment

To fit within the fairing of the original launch vehicle (Pegasus), IXPE employs a deployable optical bench, which presents challenges for alignment between optical components. The IXPE focal-plane detector has an active area of only $15 \text{ mm} \times 15 \text{ mm}$; hence each telescope must be carefully aligned to ensure that the image is near the center of the detector and that the axis of each mirror module is co-aligned with the star tracker for maximum throughput.

Ground alignment essentially consists of placing the three detectors and the three MMAs on congruent triangles, the former on the top deck of the spacecraft and the latter on the deployable mirror module support structure. This alignment is done with a laser tracker system using surface mount reflectors attached to the MMAs and the detectors. Precise knowledge linking the SMR positions to the respective nodes of the MMAs and the detectors is derived at high precision ($<50 \mu\text{m}$ for the MMAs and $<100 \mu\text{m}$ for the detectors) during component assembly. Before the MMAs are placed precisely in position, their x-ray axes are co-aligned with each other and with the optical axis of the forward-viewing star tracker using the alignment cubes.

The deployment accuracy of the boom was such that the x-ray image of an on-axis test x-ray source was within a few mm of the center of each detector when “first light” was obtained during IXPE on-orbit commissioning. For precise placement of the image, an on-board tip/tilt/rotate (TTR) system was used (Fig. 14, left). Situated between the boom and the mirror module support

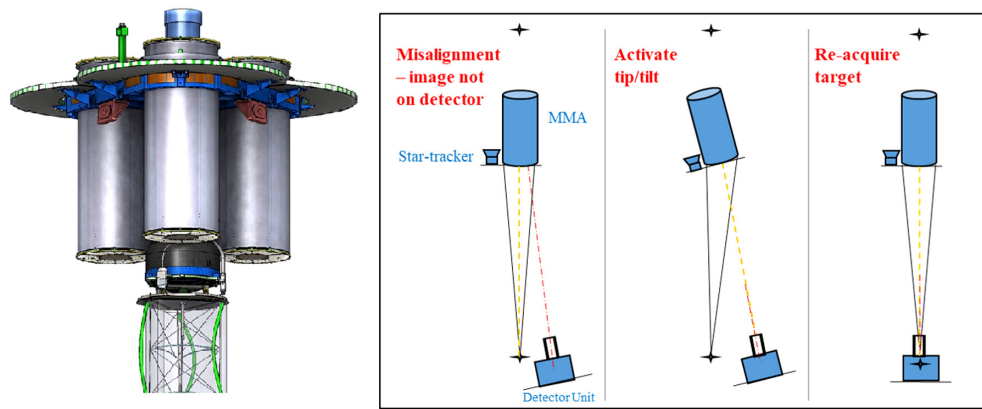


Fig. 14 Left image shows the TTR mechanism. Right image shows the MMA on-orbit alignment scheme (greatly exaggerated).

structure, the TTR can repoint the observatory to move the image on the detector as shown in Fig. 14 (right). This is possible because the star tracker is also mounted on the MMSS (see Fig. 1), so adjusting the TTR in tip/tilt has the initial effect of offset pointing the observatory, which then moves to re-acquire the target. The rotate component of the TTR can be used to compensate for any rotational offset after the boom deploys.

The combination of initial alignment and the TTR ensured that on-orbit the image was simultaneously centered on each detector (within about 30 arcsec). This is especially important for imaging polarimetry of extended sources, which are part of the IXPE observing program.

6 Summary

IXPE is a NASA small explorer mission that features three identical x-ray telescopes each consisting of a MMA with a polarization-sensitive detector at its focus. The MMAs were fabricated in-house at MSFC using an electroforming process to produce thin mirror shells, nested to provide the required collecting area. The design of the mirror system was optimized for optical and mechanical performance, factoring in thermal considerations. The challenge of assembling and aligning very-thin mirror shells while maintaining angular resolution was met with custom-designed assembly stations that monitored shell shape during integration. When completed, the MMAs were put through a series of environmental tests and were then fully calibrated. These calibrations revealed a small shortfall in effective area and angular resolution but, because of built-in margin in the requirements flow-down, the IXPE Observatory met all top-level performance requirements. IXPE was launched on December 9, 2021, and, at the time of writing, has just successfully completed its commissioning and begun its full science program.

References

1. M. C. Weisskopf et al., “The imaging x-ray polarimetry explorer (IXPE),” *Proc. SPIE* **9905**, 990517 (2016).
2. B. D. Ramsey et al., “The imaging x-ray polarimetry explorer (IXPE): technical overview IV,” *Proc. SPIE* **11821**, 118210M (2021).
3. M. C. Weisskopf et al., “Imaging x-ray polarimetry explorer: prelaunch,” *J. Astron. Telesc. Instrum. Syst.* **8**(2), 026002 (2022).
4. W. Werner, “Imaging properties of Wolter-1 type x-ray telescopes,” *Appl. Opt.* **16**, 764–773 (1977).
5. B. D. Ramsey et al., “First images from HERO, a hard-x-ray focusing telescope,” *Astrophys. J.* **568**, 432–435 (2002).
6. S. Krucker et al., “First images from the focusing optics x-ray solar imager,” *Astrophys. J.* **793**, L32 (2014).

7. M. Pavlinsky et al., “The ART-XC telescope on board the SRG observatory,” *Astron. Astrophys.* **650**, A42 (2021).
8. D. H. Lumb, N. Schartel, and F. A. Jansen, “X-ray multi-mirror mission (XMM-Newton) observatory,” *Opt. Eng.* **51**(1), 011009 (2012).
9. P. Predehl et al., “eROSITA on SRG,” *Proc. SPIE* **7732**, 77320U (2016).
10. M. Gubarev, B. D. Ramsey, and W. Arnold, “Alignment system for full-shell replicated x-ray mirrors,” *Proc. SPIE* **7360**, 73600A (2009).
11. S. Bongiorno et al., “Assembly of the IXPE mirror modules,” *Proc. SPIE* **11822**, 118220Y (2021).

Brian D. Ramsey received his PhD in astrophysics from the University of Birmingham, England, in 1978. Since 1983, he has been working in the x-ray astronomy group at the Marshall Space Flight Center. He has over 40 years of experience in experimental astrophysics, concentrating on x- and γ -ray astronomy, with over two decades of experience with x-ray optics and their associated focal plane detectors. He is currently the deputy principal investigator for the Imaging X-ray Polarimetry Explorer.

Stephen D. Bongiorno received his PhD in astrophysics from the Pennsylvania State University in 2013. He has over 10 years of experience in experimental astrophysics, currently focusing on high-resolution x-ray-optic technology development and on the alignment and environmental testing of x-ray optics for flight programs. Since 2017 he has been working in the x-ray astronomy group at the Marshall Space Flight Center, and currently serves as the lead mirror scientist for the imaging x-ray polarimetry explorer.

Biographies of the other authors are not available.